Morphological and dynamical properties of semiflexible filaments driven by molecular motors

Nisha Gupta,[1,*] Abhishek Chaudhuri,[1,†] and Debasish Chaudhuri[2,3,‡]

[1]*Indian Institute of Science Education and Research Mohali, Knowledge City, Sector 81, SAS Nagar - 140306, Punjab, India*

[2]*Institute of Physics, Sachivalaya Marg, Bhubaneswar 751005, India*

[3]*Homi Bhaba National Institute, Anushaktigar, Mumbai 400094, India*

(Received 15 August 2018; revised manuscript received 19 February 2019; published 15 April 2019; corrected 16 April 2019)

We consider an explicit model of a semiflexible filament moving in two dimensions on a gliding assay of motor proteins, which attach to and detach from filament segments stochastically, with a detachment rate that depends on the local load experienced. Attached motor proteins move along the filament to one of its ends with a velocity that varies nonlinearly with the motor protein extension. The resultant force on the filament drives it out of equilibrium. The distance from equilibrium is reflected in the end-to-end distribution, modified bending stiffness, and a transition to spiral morphology of the polymer. The local stress dependence of activity results in correlated fluctuations in the speed and direction of the center of mass leading to a series of ballistic-diffusive crossovers in its dynamics.

DOI: 10.1103/PhysRevE.99.042405

I. INTRODUCTION

The active cytoskeleton in a living cell provides its structural stability, mediates deformation and growth of the cell when necessary, and acts as transport lanes and highways for intracellular cargo [1,2]. It is made of semiflexible filaments, e.g., F-actins and microtubules, that are driven by associated motor proteins, for example, myosin and kinesin family of motor proteins, respectively [3–10]. Given the complexity of the cytoskeleton in a living cell, *in vitro* experiments were devised in which purified and stabilized cytoskeletal filaments and corresponding motor proteins were studied separately [11–17]. Single molecule experiments on motor proteins revealed details of their dynamics, e.g., force-velocity relation, dependence of turnover on load experienced, and dependence of activity on ATP concentration [5,18–24]. Motion of rigid cargo under collective drive of molecular motors has been studied both experimentally and theoretically [25–34]. In a gliding assay setup, heads of molecular motors are attached to a suitably prepared cover slit irreversibly, such that the tails can actively drive the associated filaments, hydrolyzing the chemical fuel ATP. This led to observation of collective motion, e.g., formation of spiral and aster patterns in microtubules driven by kinesin [13,35] or dynein molecules [15], or swirling patterns in high density F-actins floating on a myosin motility assay [14].

Such patterns were explained within an active hydrodynamics framework, and agent based models [14,15,36,37]. Spiral rotation and flagellalike beating of individual filaments were reproduced within effective active polymer models, modeling activity as a tangential self-propulsion [12,16,38–41], stresslets distributed over the filament contour [42,43], or chemical activity [44–46], in the presence or absence of hydrodynamic coupling. The collective dynamics in such models change from coherently free flowing motion to frozen spiraling ones with changing activity [47,48]. Generic consideration of a stiff filament in an active medium leads to the possibility of both increase or decrease of effective bending rigidity, depending on the orientation of filament segments with respect to contractile or extensile medium [49,50]. It was shown that a semiflexible filament under active correlated noise transform from bending rigidity dominated to flexible polymerlike dynamics [51]. Their center of mass motion showed a single crossover from a short time ballistic to long time diffusive behavior [40,52]. In contrast, as we show in this paper, a more microscopic consideration of both the cytoskeletal filament and motor proteins allows for local stress relaxation leading to novel behavior, e.g., a series of ballistic-diffusive crossovers of the filament center of mass.

Previous studies either modeled the motor proteins explicitly considering the driven object as a rigid cargo, or modeled the mechanical properties of the driven polymer explicitly, using self-propulsion devoid of any underlying mechanism for relaxation. Thus the impact of stress dependent dynamics of motor proteins on the filament properties, despite its importance, remains elusive within such models. In this paper we set out to address this issue. We perform numerical simulations, explicitly modeling the mechanical properties of the filament, and that of individual motor proteins as active harmonic springs undergoing attachment-detachment kinetics that do not obey detailed balance. The attachment to filament is diffusion limited, and the detachment rate increases exponentially with the extension of individual motor proteins. In the attached state the *tail* of a motor protein moves tangentially towards one end of the polymer in an active manner, with a velocity that depends nonlinearly on the motor protein extension.

We characterize the nonequilibrium conformations of the polymer comparing its end-to-end distribution with that of the

*nishagupta@iisermohali.ac.in
†abhishek@iisermohali.ac.in
‡debc@iopb.res.in

equilibrium filament. In theoretical studies of active systems, key concepts such as broken detailed balance and entropy production have recently been used to characterize the distance of these systems from their equilibrium counterparts [50,53–55]. We show that subtle changes in the local load dependence of detachment rate and active velocity of motor proteins leads to dramatic difference in the end-to-end distribution. With increasing activity, the difference increases, the effective bending stiffness reduces, and the polymer shows a phase coexistence between open and spiral chains. The most startling result is seen in the dynamics. The center of mass of the polymer shows a series of crossovers between ballistic and diffusive motion, controlled by its inertial, orientational, and speed relaxation time scales.

In Sec. II we present the model and details of the numerical simulation. All the results are discussed and analyzed in Sec. III. Finally, we present a summary and outlook in Sec. IV.

II. MODEL AND SIMULATIONS

We consider an extensible semiflexible filament described as a bead-spring chain of N beads constituting $(N-1)$ bonds of equilibrium length σ such that the chain length $L=(N-1)\sigma$, spring constant A, and finite bending rigidity κ. This is described by the Hamiltonian

$$\beta H=\sum_{i=1}^{N-1}\frac{A}{2\sigma}[\mathbf{b}(i)-\sigma\mathfrak{t}(i)]^2+\sum_{i=1}^{N-2}\frac{\kappa}{2\sigma}[\mathfrak{t}(i+1)-\mathfrak{t}(i)]^2, \tag{1}$$

with $\beta=1/k_BT$ the inverse temperature. The bond vector $\mathbf{b}(i)=\mathbf{r}(i+1)-\mathbf{r}(i)$, where $\mathbf{r}(i)$ denotes the position of the ith bead. This allows one to define the local tangent $\mathfrak{t}(i)=[\mathbf{r}(i+1)-\mathbf{r}(i)]/b(i)$. In the limit of large A, instantaneous bond lengths $b(i)\approx\sigma$, and the polymer maps to a wormlike chain [56]. In addition, excluded volume interactions between the nonbonded beads of the polymer are incorporated via a Weeks-Chandler-Anderson (WCA) potential $\beta V_{\rm WCA}(r_{ij})=4[(\sigma/r_{ij})^{12}-(\sigma/r_{ij})^6+1/4]$ if $r_{ij}<2^{1/6}\sigma$ and zero otherwise.

The polymer is placed on a substrate of motor protein (MP) assay [Fig. 1(a)]. We explicitly model MPs and their dynamics, unlike several recent studies that used effective active polymer models [40,51,52,57]. The MPs are modeled as *active* elastic linkers. We assume the MP heads are attached irreversibly to the substrate at position $\mathbf{r}_0^i=(x_0^i,y_0^i)$ placed on a two dimensional square lattice with lattice parameter a determined by the MP density ρ. The polymer floats on this MP bed. The *tails* of MPs may bind (unbind) to (from) the nearest polymer segments stochastically. The attachment process is diffusion limited. The tail of a MP attaches to a polymer segment if it lies within a capture radius r_c with an attachment rate $\omega_{\rm on}$. The extension $\Delta\mathbf{r}$ of the MP in the attached state generates an elastic load $\mathbf{f}_l=-k_m\Delta\mathbf{r}$. An attached MP unbinds from a polymer segment with a rate $\omega_{\rm off}$ which depends on the stress felt by the MP as

$$\omega_{\rm off}=\omega_0\exp(f_l/f_d), \tag{2}$$

where ω_0 is the bare off rate, $f_l=|\mathbf{f}_l|$, and f_d is the detachment force. The ratio $\omega_{\rm on}:\omega_{\rm off}$ does not obey detailed balance. When attached, a MP can move on the filament towards one of its ends, depending on the MP and filament type. For example, attached kinesin moves towards the positive end of the microtubule with *active* velocity v_t^a along the local tangent of the filament given by [22,58]

$$v_t^a(f_t)=\frac{v_0}{1+d_0\exp(f_t/f_s)}, \tag{3}$$

where $f_t=-\mathbf{f}_l\cdot\mathfrak{t}$, $d_0=0.01$, and f_s is the stall force. Here v_0 denotes the velocity of MP in the absence of stress. The extension of a given MP depends on the duration and velocity with which it moves along the filament before detachment, as well as the movement of the filament segment it is attached to. This generates a stochastic and nonuniform elastic load on different MPs.

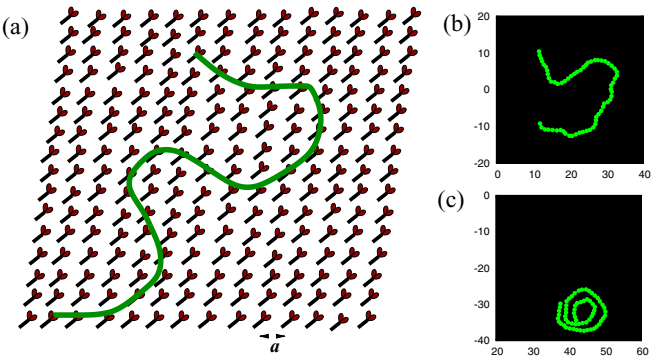

FIG. 1. (a) Schematic of the system showing the molecular motors arranged on a square grid. The semiflexible polymer glides on the bed of molecular motors. (b), (c) Simulation snapshots of the polymer in an open and spiral state for a polymer with persistence ratio $u=3.33$, under the influence of MP activity $\mathrm{Pe}=100$, and bare persistence ratio $\Omega=5/6$.

We perform numerical simulations of the model to investigate structural and dynamical properties of the polymer, actively driven by MPs. The molecular dynamics of the polymer is performed using the velocity-Verlet algorithm in the presence of a Langevin heat bath. The bath fixes the ambient temperature k_BT through a Gaussian white noise obeying $\langle\eta_i(t)\rangle=0$, and $\langle\eta_i(t)\eta_j(t')\rangle=2\alpha k_BT\delta_{ij}\delta(t-t')$, where $\alpha=3\pi\eta\sigma$ with η denoting viscosity of the environment. This defines the diffusivity over the bead size σ, $D=k_BT/\alpha$. The units of energy, length, and time are set by k_BT, σ, and $\tau=\alpha\sigma^2/k_BT$, respectively.

We set out to perform numerical simulations to study conformational and dynamical properties involving the longest length and time scales of the polymer, under the influence of an active MP bed pumping energy from the shortest length scales. The large separation between length and time scales makes a fully microscopic parametrization of molecular motors prohibitively expensive in terms of simulation time. For example, the capture radius is expected to be a fraction of the size of the molecular motor, i.e., $\sim$10 nm. This is three to four orders of magnitude smaller than the typical filament lengths that are used in MP assays. On the other hand, the longest relaxation time of a semiflexible filament of length L varies as $\sim L^4$ [59]. To keep the calculations tractable, we choose a capture radius $r_c=0.5\sigma$, smaller than

the unit of length in the model, to be qualitatively consistent with the fact that this should be the shortest length scale of the problem. The active forces associated with MPs are known to be larger than that coming from thermal fluctuations, and we use $f_s = 2k_BT/\sigma$ and $f_d = f_s$. The coarse-grained nature of the polymer segments considered allows multiple MPs to get associated with them, captured by our somewhat large MP density in the 2D assay, $\rho = 3.8\sigma^{-2}$. The large spring constant $A = 100\sigma^{-1}$ is chosen to keep the bond length fluctuations small (within 5%). In the absence of direct measurement of effective spring constant of active MPs (we are not considering the rigor bonds), we have chosen $k_m = A/\sigma$ for simplicity. The attachment (detachment) of MP tails are stochastic and performed using probabilities $\omega_{\rm on}\delta t$ ($\omega_{\rm off}\delta t$). The extension in the attached state has two contributors—the MP tail is dragged along with the filament segment to which it is attached and it can slide from one segment to another with an active velocity v_t^a. We study the influence of the active bed of MPs on the static and dynamic properties of the polymer as we vary the (a) bare processivity $\Omega = \omega_{\rm on}/(\omega_{\rm on} + \omega_0)$ and (b) a dimensionless Péclet number defined as ${\rm Pe} = v_0\sigma/D$. The numerical integrations are performed using $\delta t = 10^{-3}\tau$ for ${\rm Pe} = 1$ and $\delta t = 10^{-4}\tau$ for ${\rm Pe} = 10, 100$. Unless stated otherwise, we use $\Omega = 5/6$, which corresponds to kinesin MP property $\omega_{\rm on} : \omega_0 = 5 : 1$ [60–62]. The simulations are done over 2×10^9 steps, and the steady state measurements are presented over 10^6 configurations separated by 10^3 steps, discarding the first 10^9 steps.

III. RESULTS

At equilibrium, mechanical and structural properties of a semiflexible filament are determined by the persistence ratio $u = L/\lambda$, where L is the contour length of the chain, and $\lambda = 2\kappa/(d-1)$ is the persistence length, where $d = 2$ is the dimensionality of the embedding space [56]. The active drive from processive MPs attaching (detaching) to (from) the filament generates nonequilibrium stress which has a profound effect on the steady state conformational properties of the polymer. To characterize the conformational properties, we obtain probability distribution of the end-to-end distance, $P(r, L)$, of the polymer. At equilibrium, this has the scaling form $P(r, L) = \frac{1}{L^d}p(r/L, L/\lambda) = \frac{1}{L^d}p(\tilde{r}, u)$, where $\tilde{r} = r/L$ and $u = L/\lambda$. The limits of $u \to 0$ and ∞ are the limits of rigid rod and flexible polymers, respectively. For an equilibrium wormlike chain, $p(\tilde{r}, u)$ shows a first-order-like transition from a single maximum at $\tilde{r} = 0$ for the flexible limit of large u to a maximum at $\tilde{r} = 1$ for a very rigid polymer with small u [56,63]. We choose the value of $u = 3.33$, in the regime between these two limits where semiflexibility is most strongly pronounced [63], to examine the impact of an active MP bed on semiflexible polymers. In *in vitro* experiments, the ratio u may be tuned by controlling persistence length of the chain by, e.g., changing salt concentration in the medium thereby changing interaction, or by stabilizing the chain lengths. In all our simulations, unless stated otherwise, for $L = 63\sigma$ chains, $u = 3.33$ sets $\lambda = 18.92\sigma$. Two typical configurations of the MP driven polymer are shown in Figs. 1(a) and 1(b) for ${\rm Pe} = 100$ and $\Omega = 5/6$.

A. How far from equilibrium is the polymer morphology?

Under the active drive of the gliding assay of MPs, the morphology of the polymer changes. In Fig. 2 we show how this impacts the end-to-end distribution function $p(\tilde{r}, u)$. The conformational change with respect to the equilibrium is well captured by the logarithmic ratio,

$$\Delta\Sigma = \ln\left[\frac{p(\tilde{r})}{p_{\rm eq}(\tilde{r})}\right]. \tag{4}$$

In Fig. 2(a) we show how the dimensionless quantity $\Delta\Sigma$ changes with activity. For comparison, the equilibrium distribution $p_{\rm eq}$ is shown in Fig. 2(c).

If the activity of MPs is independent of the load force acting on them, $\omega_{\rm off} = \omega_0$ and $v_t^a = v_0$. This corresponds to the limit of infinitely large f_d and f_s. It is expected that the deviation $\Delta\Sigma$ would be large for large nonequilibrium driving, quantified in terms of f_d, f_s, and Ω. In Fig. 2, we explore the impact of activity using the moderate value of ${\rm Pe} = 1$.

We first consider the situation in which $\omega_{\rm off} = \omega_0$ is kept fixed so that $\Omega = 5/6$, and the active velocity v_t^a is varied [Fig. 2(a)] for three possible situations. (i) In the absence of any directed motion of the polymer, i.e., with $v_0 = 0$, $\Delta\Sigma$ shows a dip near $\tilde{r} = 0$, indicating a relative bias to the *open* conformations of the polymer. This indicates that a mere stochastic attachment or detachment kinetics of MPs, that does not obey detailed balance, leads to an enhancement of effective stiffness of the filament. (ii) When attached, MPs move, and if the active velocity is assumed to be *independent* of the load experienced, we use $v_t^a = v_0$. The effect is dramatic. The filament, gliding on the attached MPs, undergoes a transition to a rotating spiral configuration (discussed further in Sec. III D). This gives rise to a peak in $\Delta\Sigma$ near $\tilde{r} = 0.1$. (iii) If we incorporate local stress dependence in v_t^a, the polymer is still softened but now switches between gliding and spiral states more freely. Thus, in addition to the peak near $\tilde{r} = 0.1$, a nonzero value at higher $\tilde{r}$ appears in $\Delta\Sigma$. The statistics, dynamics, and mechanical properties of the polymer under MP drive is determined by a competition between processive active velocity of MPs and bending stiffness of the polymer.

We next consider the situation allowing the detachment rate $\omega_{\rm off}$ to be *dependent* on the load force felt by individual MPs [Eq. (2)]. Given their similarity with the equilibrium distribution, $\Delta\Sigma \approx 0$ [Fig. 2(c)], the corresponding nonequilibrium end-to-end distributions are shown explicitly in Fig. 2(b). The nonequilibrium stress buildup due to activity is relaxed easily by enhanced unbinding rate of stretched MPs allowing the polymer morphology to adopt equilibriumlike conformations. The distribution is closest to equilibrium for $v_t^a = 0$. The strongest nonequilibrium feature is observed at stress *independent* activity $v_t^a = v_0$. At this point the distribution clearly shows a bimodality with two maxima at $\tilde{r} \approx 0, 0.8$. Consideration of the stretching dependent decrease of active velocity as in Eq. (3) decreases the height of the flexible chain maximum at $\tilde{r} \approx 0$, as the polymer switches between gliding and spiral states more easily.

In most biologically relevant situations, both the turnover and active motion of individual MPs depend on their instantaneous extension. The activity is most strongly reflected in terms of the bare velocity of MPs v_0. As was shown in

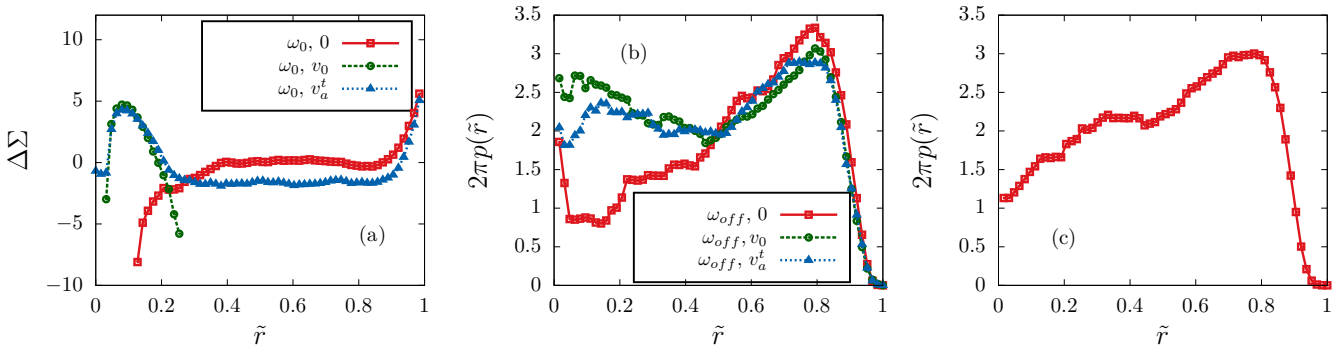

FIG. 2. Activity dependence of end-to-end distribution functions and their difference from equilibrium for a filament with $N = 64$ having persistence ratio $u = 3.33$. The MP activity is controlled by turnover with a bare processivity $\Omega = 5/6$, and nonzero active velocity v_0 set by $\mathrm{Pe} = 1$. (a) The logarithmic ratio of probabilities of filament under active drive with respect to that of the equilibrium polymer, $\Delta\Sigma$, provides a measure of the difference in distributions. The legends denote parameter values (detachment rate, MP velocity), where, in this figure, all data sets correspond to a constant detachment rate ω_0 and MP velocity varies between constant values zero, v_0, and stretching dependent active velocity v_t^a as denoted by Eq. (3). (b) The end-to-end distribution of stretchable semiflexible polymer $p(\tilde{r})$, with local strain dependent detachment ω_{off} as in Eq. (2). (c) The end-to-end distribution of the stretchable semiflexible polymer at equilibrium $p_{\mathrm{eq}}(\tilde{r})$.

Ref. [22], this velocity of unloaded kinesin MP increases from 1 nm/s to finally saturate to $\sim$1 μm/s, as the ambient ATP concentration increases from 1 μM to 1 mM. The change in v_0 is captured by changing Pe in our current setup. In Fig. 3, we show how polymer properties vary with increasing Pe when both ω_{off} and v_a^t are treated as local strain dependent quantities. For low values of Pe, the local forces acting on the polymer backbone due to binding kinetics and motor movement are not sufficient to cause significant local curvature. As Pe is increased, due to tangential velocity of MPs and enhanced directional fluctuations, the polymer starts to coil up and rotates with a spiral configuration in the steady state (discussed further in Sec. III D). The impact shows up in terms of a maximum in $p(\tilde{r})$ near $\tilde{r} = 0.2$ appearing for large Péclet, $\mathrm{Pe} = 100$ (Fig. 3). This feature is robust with respect to change in Ω (see Appendix A).

B. Competition between activity and bending stiffness

For a semiflexible polymer in equilibrium, the end-to-end distribution $p(\tilde{r}, u)$ is determined by the dimensionless ratio $u = L/\lambda$. On the other hand, in the presence of motor proteins,

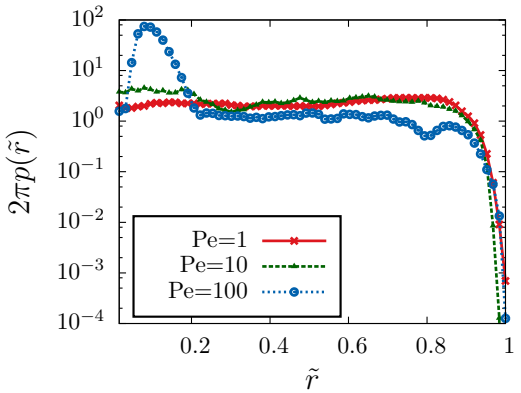

FIG. 3. End-to-end distribution for three different values of Pe using stretching dependent turnover ω_{off}. All other parameters are as in Fig. 2.

the statistical and mechanical properties are expected to be determined by an interplay of activity and bending rigidity. To probe that within our model, here we fix $\omega_{\mathrm{off}} = \omega_0$, and vary the chain length $L = (N-1)\sigma$ by changing N, the ratio $u = L/\lambda$, and persistence length λ of the polymer to study their impact on conformational properties. We use both stress dependent and independent v_a^t, and plot the end-to-end distributions for three different active velocities in Fig. 4. A comparison of Figs. 4(a) and 4(b) clearly shows that, for the same u and different L, unlike in equilibrium semiflexible chains, the conformational properties of the polymer are significantly different. For example, for $N = 128$ and $u = 3.33$ [Fig. 4(b)], the distribution for $v_0 = 0$ indicates a much stiffer polymer compared to $N = 64$ [Fig. 4(a)]. For nonzero active velocity, the spiral states observed for $N = 64$ disappear for $N = 128$, leading to stiffer conformations devoid of spirals. If, however, we keep the value of λ fixed as we change the length of the polymer from $N = 64$ to $N = 128$ [Fig. 4(c)], the distributions we get compare much better with Fig. 4(a). This suggests that, for a given processivity Ω, the conformational properties of polymers driven by MPs are determined by a competition between active velocity and bending rigidity, and not by the ratio u.

Within active polymer models with constant tangential drive, arguing that active force f_p may generate compression, a torque balance leads to a critical active force $f_p^c \sim \lambda/L^3$, beyond which straight filaments are unstable towards buckling [41]. In the limit of stress independent activity, a simple extension of this relation to the instability of the filament under MP driving can be obtained by replacing $f_p^c = \alpha\Omega v_0^c$. This leads to a relation $v_0^c \sim \lambda/\alpha\Omega L^3$. Thus buckling instabilities are expected to be controlled by the dimensionless number $\mathcal{F} = \alpha\Omega v_c L^3/\lambda$. However, for polymers driven by real MPs that show stress dependent activity and turnover, the determining factors turn out to be more subtle.

C. Determination of effective stiffness

To further characterize the steady state conformational properties of the polymer, we consider the tangent-tangent

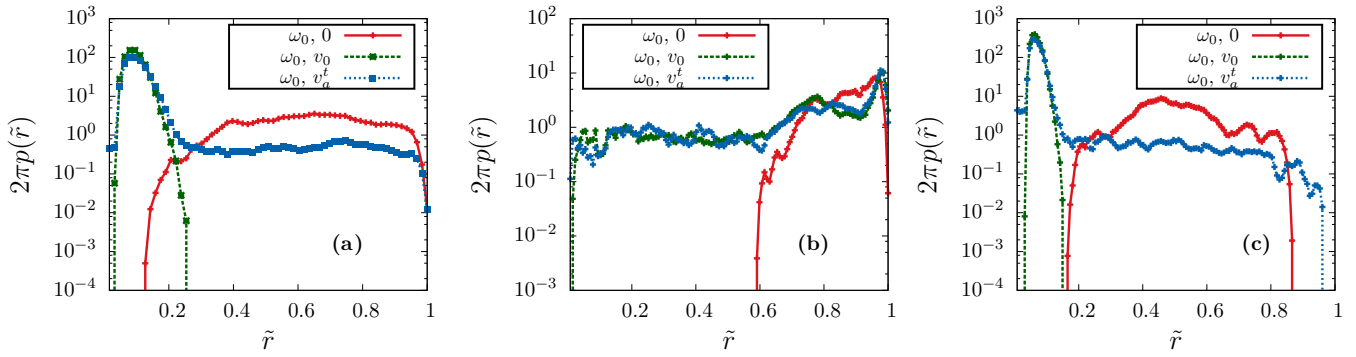

FIG. 4. End-to-end distribution functions. We use constant detachment rate ω_0 with $\Omega = 5/6$ for all the figures. The variation of MP active velocities are as in Fig. 2, with the nonzero active velocities set by $\mathrm{Pe} = 1$. The three graphs show results for (a) $N = 64$, $u = 3.33$, $\lambda = 18.92\sigma$, (b) $N = 128$, $u = 3.33$, $\lambda = 38.14\sigma$, and (c) $N = 128$, $u = 6.66$, $\lambda = 18.92\sigma$.

correlation function, $\langle \mathrm{t}(s) \cdot \mathrm{t}(s') \rangle$ for different Pe. For an equilibrium wormlike chain, one expects a single exponential decay of the correlations, characterized by the persistence length λ, as $\langle \mathrm{t}(s) \cdot \mathrm{t}(s') \rangle = \exp(-|s - s'|/\lambda_{\mathrm{eff}})$. In the long separation limit, the presence of self-avoidance leads to an effective power law correlation function determined by the Flory exponent, a behavior we ignore for relatively short length scales in the ensuing discussion. This results in a λ_{eff} that is larger than λ in equilibrium simulations. The tangent-tangent correlation provides a measure for structural rigidity of the filament and can be determined from experiments by fluorescent imaging of polymer conformations. In Fig. 5, we observe that the correlation function for small activity, $\mathrm{Pe} = 1$, shows a characteristic exponential decay that follows the equilibrium correlation function very closely. Figure 5 shows that the correlation length decreases with increase in Pe. This is indicative of a softening of the polymer with the emergence of strong bending fluctuations. Up to $\mathrm{Pe} = 10$ shown in the graph, the overall nature can be described by a single exponential decay, which is fitted to extract the effective persistence length λ_{eff}, directly. For higher values of Pe, e.g., at $\mathrm{Pe} = 100$, the correlations start showing oscillations, capturing emergence of spiral conformations that occur at higher activity. In such cases, the crossing of zero by the correlation function is interpreted as the persistence length. The variation of this effective persistence length with activity is listed in Table I.

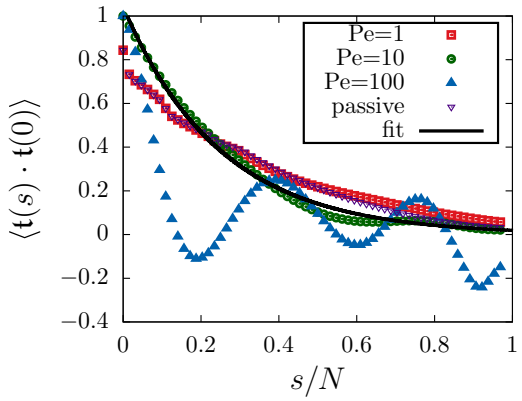

FIG. 5. Tangent-tangent correlation function for a chain of $N = 64$, $u = 3.33$, and activity v_t^a set by $\mathrm{Pe} = 1$, 10, and 100 and load dependent detachment rate ω_{off} with $\Omega = 5/6$. The data set *passive* denotes equilibrium result. The solid line shows a single exponential fit to $\mathrm{Pe} = 10$ data used to extract the effective persistence length $\lambda_{\mathrm{eff}} = (15.99 \pm 0.24)\sigma$.

D. Coexistence of spiral and open chains

In order to quantify the observations of the different conformational states of the polymer, we use the turning number [64], $\psi(s) = (1/2\pi) \int_0^s ds' (\partial\vartheta/\partial s')$, where $\vartheta(s)$ is the angle subtended by the unit tangent $\hat{t}(s)$ with x axis. This $\psi(s)$ is a good order parameter, clearly distinguishing an open polymer from a spiral one and also separating clockwise and counterclockwise spiral states [Fig. 6(a)]. The steady state probability distribution of $\psi(s = L)$ is a Gaussian with a peak at $\psi(L) = 0$ for small Pe, indicating the absence of spiral states. Increasing Pe has a dramatic effect on the distribution, with symmetric peaks emerging for nonzero $\psi(L)$ indicative of coexisting spiral states with equal probabilities of clockwise and counterclockwise winding, along with the open state characterized by $\psi(L) = 0$. Such phase coexistence is a characteristic feature of a nonequilibrium first order phase transition. Similar coexistence of spiral and open conformations were observed earlier in an active polymer model characterized by constant tangential force [40]. It was not *a priori* clear that our current model would give rise to a similar conformational behavior, given that the activity in our model gets modified by the buildup and release of local strain via load dependent activity and turnover. As we have already

TABLE I. Activity modulated effective persistence length of a chain of length $L = 63\sigma$ (with $N = 64$) and $\lambda = 18.92\sigma$. The table shows λ_{eff} obtained from tangent-tangent correlation function. With Pe, the persistence length first increases and then decreases.

Pe	$\lambda_{\mathrm{eff}}/\sigma$
Equilibrium	23.59 ± 0.39
1	25.21 ± 0.23
10	15.99 ± 0.24
100	8.89

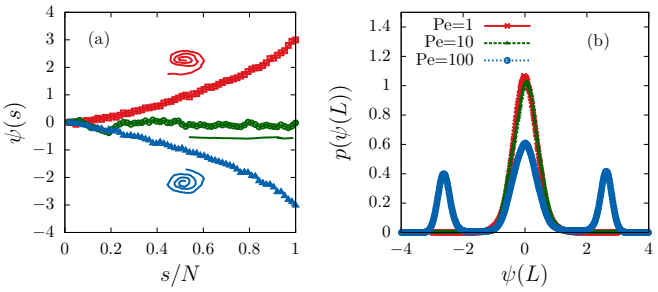

FIG. 6. Analysis of the turning number $\psi(s)$ using $N = 64$, $u = 3.33$ and load dependent detachment ω_{off} with $\Omega = 5/6$ with activity v_t^a set by Pe. (a) Plot of $\psi(s)$ for three different configurations with Pe $= 100$. It shows that $\psi(s)$ is an effective order parameter, distinguishing between the open state (green), clockwise spiral (blue), and counterclockwise spiral (red). (b) Probability distributions for $\psi(L)$ at Pe $= 1$, 10, and 100.

shown, in fact, the effect of local strain dependence reflects strongly in the end-to-end distribution functions $p(\tilde{r})$. Further, as we show in the following section, this implies dynamical crossovers in mean squared displacement that are unlike the active polymer model.

E. Anomalous dynamics of the center of mass

In Fig. 7(a) we show mean squared displacement (MSD) of the polymer center of mass as a function of time, for three different Pe values that are separated over two decades. At very short time scales the MSD shows an approximate *ballistic* scaling $\langle \Delta r_{\text{cm}}^2 \rangle \sim t^2$ up to $t \approx 1$ at all Pe. With increasing time, five crossovers at Pe $= 1$ can be clearly seen; these include three ballistic-diffusive crossovers and two diffusive-ballistic crossovers. At Pe $= 10$, numerical integration required a smaller step size restricting the results to a shorter total time t. Otherwise, all the crossovers are retained at Pe $= 10$, with a reduction in crossover times. The qualitative behavior changes as the activity is increased to a larger value, Pe $= 100$. At this regime the first ballistic-diffusive crossover almost vanishes. At $t \approx 1$ one finds a barely discernible change in the slope which quickly gets back to ballistic scaling. This is due to an effective merger of the first diffusive-ballistic crossover to the first ballistic-diffusive one. The ballistic-diffusive crossovers discussed in this section are a recurring feature of active systems [40,52,65,66]. It is known that a persistent random walker undergoes a crossover from initial ballistic to a final diffusive motion, while directed random walkers show a crossover from short time diffusive to long time ballistic scaling [65]. In the following section we present a detailed explanation of the crossovers observed.

In Fig. 7(b), we show time evolution of the center of mass position of the polymer at Pe $= 100$, indicating its various conformations associated with the trajectory. As the polymer takes a folded conformation, which is often a spiral in our system, the force generated in different segments by the gliding assay cancel each other and the net directed force on the center of mass is negligible. As a result, the center of mass moves diffusively, getting mostly localized in a narrow region, albeit with an enhanced diffusivity. When the polymer retains a more open conformation, the gliding assay indeed generates directed force on the center of mass, leading to a ballistic motion over such periods shown by long directed trails.

More quantitatively, the ballistic-diffusive crossovers are associated with changes in the evolution of the end-to-end extension r_{ee}, the orientation of the end-to-end vector ϕ, and the root mean squared (rms) fluctuation of the center of mass position $\sqrt{\Delta r_{\text{cm}}^2}$ along a single trajectory. In Fig. 7(c) we show this at Pe $= 100$. Clearly there are time spans over which r_{ee} remains close to zero, i.e., the polymer remains in a folded (spiral at Pe $= 100$) state, e.g., between $t \approx 4.5$–$5 \times 10^5\,\tau$. It should be noted that the formation of spiral happens at high Pe, as was shown in Sec. III D. However, even at smaller Pe, the chain switches between open and nonspiral folded conformations. Nonspiral folds show a little higher value of r_{ee} than when spirals form. There are other time windows over which r_{ee} fluctuates rapidly between open and spiral states (e.g., between $t \approx 0$–$4 \times 10^5\,\tau$).

As is shown in Fig. 7(c), ϕ changes ballistically on a time span over which r_{ee} remains close to zero in a spiral state. In particular, between $t = t_1$ and t_2 the spiral rotates

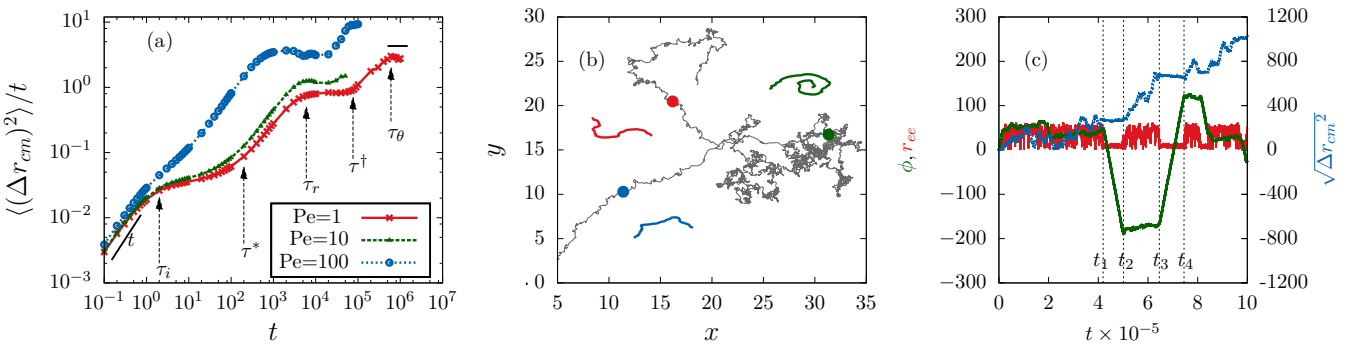

FIG. 7. Dynamics of center of mass for a chain of $N = 64$, $u = 3.33$, with load dependent MP activity v_t^a controlled by Pe and detachment rate ω_{off} determined by $\Omega = 20/21$. (a) Mean squared displacement of the center of mass at different Péclet (Pe $= 1$, 10, 100). Numerical analysis of the dynamics at Pe $= 100$ is presented in (b) and (c). (b) The gray line shows a center of mass trajectory. Structure of polymer corresponding to the blue, red, and green points indicated on the trajectory are shown in the respective colors. (c) The end-to-end length r_{ee} (red line), end-to-end orientation ϕ (green line), and root mean squared fluctuations of the center of mass position (blue line) for a single trajectory are shown as a function of time at Pe $= 100$.

clockwise ballistically reflected in a linear change in ϕ with a negative slope. During such time spans, the r_{ee} of spirally folded polymer remains small, and the center of mass position of the polymer does not change appreciably, as is shown by the flat segment of $\sqrt{\Delta r_{cm}^2}$ in Fig. 7(c) in this time window. In the window of $t = t_2$ and t_3 the filament opens up switching between relatively close and open conformations stochastically captured by the strong fluctuations in r_{ee}. In such a state the directed rotation practically stops, captured by the flat, approximately parallel to t-axis portion of the $\phi(t)$ curve. The polymer encounters directed drive from MPs during the time spans over which it opens up leading to appreciable displacement $\sqrt{\Delta r_{cm}^2}$ of the center of mass. Between $t = t_3$ and t_4, the polymer folds back into a spiral state again, and starts rotating in the *counterclockwise* direction this time, captured by the linear increase in ϕ, associated with characteristic flat segments of r_{ee} and $\sqrt{\Delta r_{cm}^2}$.

F. Ballistic to diffusive cross overs

To analyze the crossovers of the center of mass MSD, let us first consider the dynamics of a particle in a Langevin heat bath in the absence of any active drive, $m\,dv/dt = -\alpha v + \eta(t)$, where the Gaussian random noise obeys $\langle \eta(t)\rangle = 0$ and $\langle \eta(t)\eta(0)\rangle = 2\alpha k_B T \delta(t)$. The corresponding displacement fluctuation of passive origin is given by

$$\langle \Delta r_p^2(t)\rangle = 6\frac{k_B T}{m}\tau_I^2\left[\frac{t}{\tau_I} - 1 + e^{-t/\tau_I}\right], \tag{5}$$

where $\tau_I = m/\alpha$. For time scales $t \ll \tau_I$ this leads to a ballistic scaling of MSD, $\langle \Delta r_p^2(t)\rangle \approx 3v_{eq}t^2$, with a velocity $v_{eq} = (2k_BT/m)^{1/2}$. At longer times $t \gtrsim \tau_I$, this crosses over to a diffusive scaling $\langle \Delta r_p^2(t)\rangle = 6D_{eq}t$ with $D_{eq} = k_BT/\alpha$. As is shown in Fig. 7(a), the polymer center of mass shows such a crossover near $\tau_I = 1$ in our simulations [67].

Because of the molecular motor drive, further ballistic-diffusive crossovers beyond t_I are observed. Following Ref. [65], we identify two possible mechanisms related to activity: (i) the persistence of the direction of center of mass velocity described by the correlation time τ_θ and (ii) the correlated fluctuations of the speed of the center of mass with correlation time τ_s. The speed fluctuations are approximately captured by an exponential correlation $C_{v_s}(t) = \langle \delta v_s(t)\delta v_s(0)\rangle/\langle \delta v_s^2\rangle \approx \exp(-t/\tau_s)$ where $\delta v_s = v_s - \langle v_s\rangle$ (Fig. 9 in Appendix B). Similarly, the orientational fluctuation of velocity obeys $C_\theta(t) = \langle e^{i[\theta(t)-\theta(0)]}\rangle \approx \exp(-t/\tau_\theta)$, where τ_θ is the persistence time (Fig. 10 in Appendix B). On the other hand, as we find, the velocity amplitude and orientations are only weakly correlated (Fig. 11 in Appendix B). Such correlations can be ignored to use the expression of active displacement fluctuations,

$$\langle \Delta r^2(t)\rangle = \langle \Delta r_p^2(t)\rangle + 2\langle v_s\rangle^2\tau_\theta^2\left(\frac{t}{\tau_\theta} - 1 + e^{-t/\tau_\theta}\right) + 2\langle \delta v_s^2\rangle\tau_r^2\left[\frac{t}{\tau_r} - 1 + e^{-t/\tau_r}\right], \tag{6}$$

where $\tau_r^{-1} = \tau_\theta^{-1} + \tau_s^{-1}$. In the above expression the speed $\langle v_s\rangle$ and its fluctuations $\langle v_s^2\rangle$ are due to activity controlled by Pe. If $\langle \delta v_s^2\rangle = 0$, the above expression would suggest a ballistic dynamics for $t \ll \tau_\theta$, crossing over to diffusion at $t \gtrsim \tau_\theta$ as the direction of persistent motion diffuses. This is expected for structureless active Brownian particles with constant active speed.

However, in the presence of speed fluctuations in the polymer, the other time scale $\tau_r < \tau_\theta$ intervenes. The total mean squared displacement of the polymer center of mass has contributions from both thermal fluctuations Eq. (5) and activity Eq. (6). If the three time scales $\tau_I \ll \tau_r \ll \tau_\theta$ present in the problem are well separated, they are expected to lead to three ballistic-diffusive crossovers. (a) At $t \ll \tau_I$ one expects a ballistic motion $\langle \Delta r_{cm}^2\rangle \approx 3v_{eq}t^2$ with a velocity $v_{eq} = (2k_BT/m)^{1/2}$. (b) At $t \gtrsim \tau_I$ one crossover to diffusive regime takes place, with equilibrium diffusion constant $D_{eq} = k_BT/\alpha$. This is the first ballistic-diffusive crossover, and is independent of activity. (c) This regime lasts until $\tau^* = 3(v_{eq}^2/\langle \delta v_s^2\rangle)\tau_I$ at which the chain starts to respond to the active force that drives it in a directed manner. This gives rise to the first diffusive-ballistic crossover. For $\tau^* < t \ll \tau_r$, we find a ballistic behavior dictated by the active speed fluctuation $\sim\langle \delta v_s^2\rangle t^2$. A sufficiently strong activity can enhance $\langle \delta v_s^2\rangle$ to reduce τ^* to merge this active ballistic regime to the equilibrium ballistic scaling, as is seen for Pe = 100 in our simulations. (d) As t crosses τ_r, the scaling of $\langle \Delta r^2(t)\rangle$ crosses over to another diffusive regime, the second ballistic-diffusive crossover, with effective diffusion constant $D \approx D_{eq} + \frac{1}{3}\langle \delta v_s^2\rangle\tau_r$. (e) This regime persists until $\tau^\dagger = 3(v_{eq}^2/\langle v_s\rangle^2)\tau_I + 2(\langle \delta v_s^2\rangle/\langle v_s^2\rangle)\tau_r$. Beyond this point the second diffusive-ballistic crossover takes place. For $\tau^\dagger < t \ll \tau_\theta$, the ballistic behavior is dictated by $\sim\langle v_s\rangle^2 t^2$. (f) For $t \gtrsim \tau_\theta$, this ballistic regime slowly crosses over to the final diffusive behavior, the third ballistic-diffusive crossover, dictated by an effective diffusion constant $D \approx D_{eq} + \frac{1}{3}(\langle \delta v_s^2\rangle\tau_r + \langle v_s\rangle^2\tau_\theta)$. This qualitatively explains the ballistic-diffusive crossovers obtained in Fig. 7(a).

Before ending this section, we note that the fluctuations in active speed and orientation in the polymer arise essentially from the same driving mechanism due to molecular motors and conformational relaxation of the polymer. Thus the two quantities may have similar fluctuations and significant cross correlation. In Appendix B we show the autocorrelation functions of the center of mass speed and the active orientation, as well as the cross correlation between the two. The autocorrelation data show longer correlation times for the orientational fluctuations. The cross-correlation function breaks time-reversal symmetry, capturing the nonequilibrium driven nature of the system, and shows correlation even at long time gaps.

IV. DISCUSSION AND OUTLOOK

Using stochastic molecular dynamics simulations we have investigated the conformational and dynamical properties of a semiflexible polymer in the presence of motor proteins, which (un)bind (from) to the polymer and perform directed active motion. Unlike in the equilibrium wormlike chain, the end-to-end statistics in this case is not controlled by the ratio of persistence length and chain length, but results from a local competition between the processive active velocity and bending rigidity. As is shown in this paper, local stress dependence

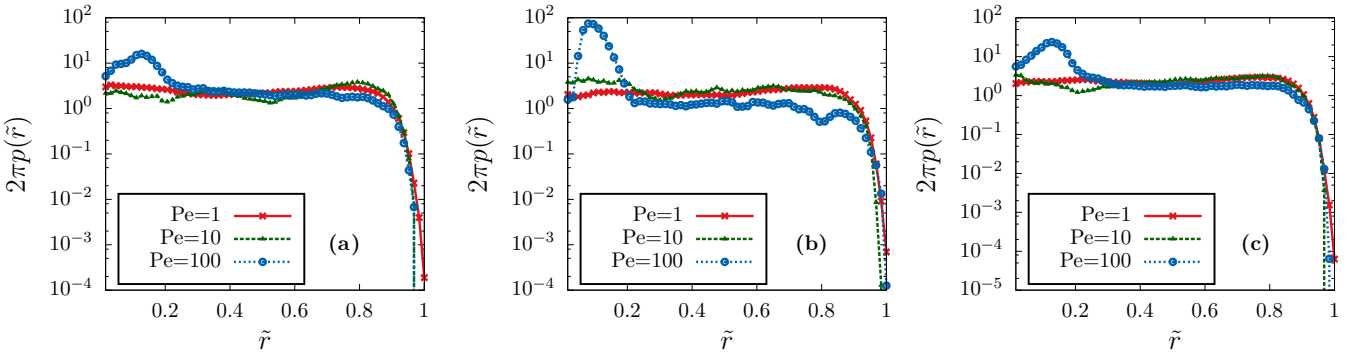

FIG. 8. End-to-end distribution at Pe = 1, 10, 100 for different values of bare processivity Ω, using stress dependent active velocity and detachment rate with $N = 64$, $u = 3.33$. The graphs correspond to (a) $\Omega = 2/3$, (b) $\Omega = 5/6$, and (c) $\Omega = 20/21$.

of turnover and active velocity provides new relaxation mechanisms giving rise to steady states unlike the active polymer models with constant tangential self-propulsion. The activity influences polymer morphology, mechanical properties, and dynamics in a concerted manner. With increasing activity of the motor proteins, we observed the following. (i) The end-to-end distribution characterizing polymer conformation shows both stiffening and softening relative to the equilibrium morphology associated with the buildup of local active stress and its relaxation. (ii) The stretching dependent active velocity and turnover of molecular motors gives rise to an interplay of three time scales, the inertial, orientational, and speed relaxation times of the center of mass, leading to a series of ballistic-diffusive crossovers in the mean squared displacement of the center of mass.

These crossover time scales can be interpreted into real times using dynamics of a filament of ∼2 μm length. For example, considering $\sigma = 20$ nm, the 64 bead chain can be interpreted to have a length 1.84 μm. This sets $f_s = f_d = 0.4$ pN, slightly smaller than the pN scale in, e.g., kinesin molecules. Assuming the viscosity of ambient fluid 100 times that of water, i.e., equivalent to that in cytoskeleton [1], one obtains a viscous drag of $\alpha = 0.02$ pN s/μm. This sets the unit of time $\tau = 0.002$ s. As expected, only the noninertial time scales are relevant from the perspective of slow dynamics. Interpreting the predictions from Fig. 7(a) we find the following slow time scales: the ballistic-diffusive crossover times $\tau_r \sim 15$ s, and $\tau_\theta \sim 15$ min, and the diffusive-ballistic crossover time $\tau^\dagger \sim 3$ min. The predictions presented here are amenable to verification in experiments on molecular motor assays.

While our system reproduces some of the predictions of the standard active polymer model, some other properties that we observe are entirely due to the strain dependence of the activity and turnover of MPs. For example, the observed activity dependent reduction of effective bending stiffness and the coexistence of spiral and open conformations at an activity beyond a critical value are expected within the active polymer model. On the other hand, the detailed nature of end-to-end distribution functions and the series of ballistic-diffusive crossovers observed in the center of mass dynamics are features that are unlike active polymer models [40].

ACKNOWLEDGMENTS

A.C. and D.C. acknowledge SERB, India for financial support through Grant No. EMR/2014/000791. D.C. thanks SERB, India, for financial support through Grant No. EMR/2016/001454, and ICTS-TIFR, Bangalore for support through an associateship. N.G. acknowledges UGC, India for support through a fellowship.

APPENDIX A: END-TO-END DISTRIBUTIONS FOR DIFFERENT Ω

In Fig. 8, we show the dependence of the conformational properties of the polymer as the bare processivity $\Omega = \omega_{\rm on}/(\omega_{\rm on} + \omega_0)$ is varied. Here we consider the scenario where both the detachment rate and the active velocity depend on the local stress. For a fixed Ω we plot the end-to-end distribution of the polymer as Pe is changed. As in Fig. 2(c), the distributions look similar to equilibrium distribution $p(\tilde{r})$ for low Pe and a peak near $\tilde{r} \approx 0$ appears for high Pe, indicating the emergence of spiral states. Therefore, we conclude that, for stress dependent $\omega_{\rm off}$, varying Ω does not affect the conformational properties significantly. Recall that a stress

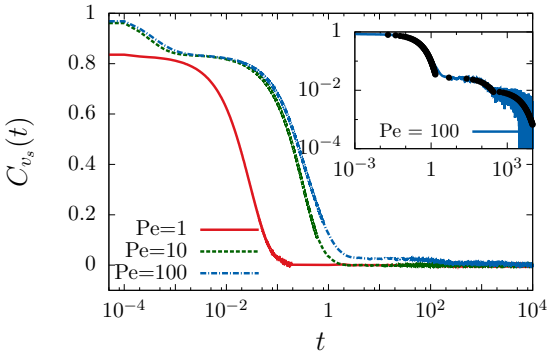

FIG. 9. Speed autocorrelation of the center of mass of the polymer. Single exponential decays are observed for both Pe = 1, 10, with correlation times $t_s \approx 0.1\tau, 1.0\tau$, respectively. (Inset) In the log-log plot, for Pe = 100, multiple exponential decays with $t_s \approx 1\tau, 250\tau, 2000\tau$ are shown. The three exponential fits are indicated by black points.

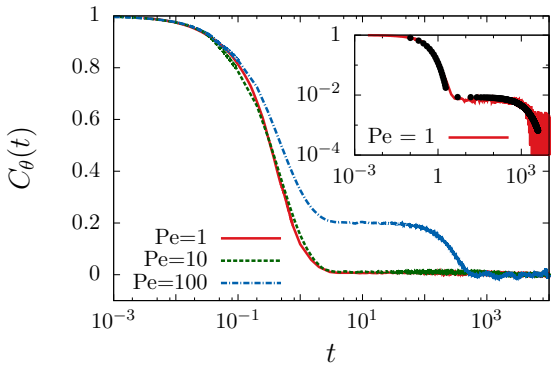

FIG. 10. Orientational autocorrelation of the center of mass velocity vector. This shows multiple exponential decays for all Pe. (Inset) For Pe = 1, the log-log plot shows multiple exponential decays with time scales $t_\theta \approx 1\tau, 1500\tau$. The two exponential fits are indicated by black points.

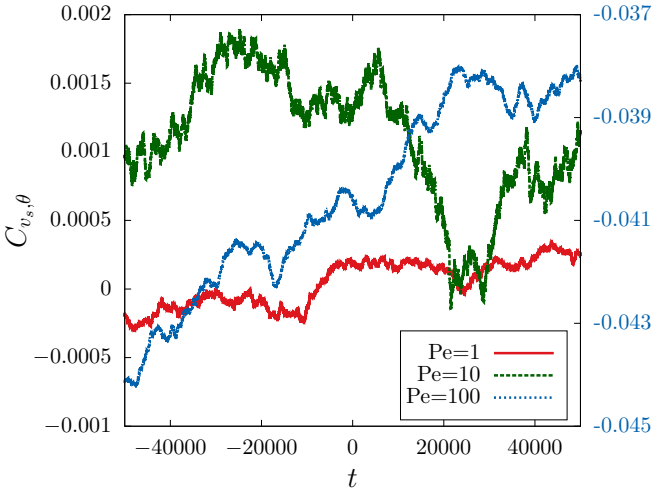

FIG. 11. Cross correlation of the orientation and speed of the center of mass velocity for Pe = 1 (red), 10 (green), and 100 (blue, and values correspond to right ordinate).

independent ω_{off} with nonzero Pe results in coiled states of the polymer. Switching on local stress dependence in ω_{off} allows the polymer to relax back to its equilibrium conformations whenever stress builds up beyond a limit, even if the processivity Ω is high. As Pe is increased, it triggers an instability towards spiral states and we see the emergence of a peak near $\tilde{r} = 0$ in the steady state distributions.

APPENDIX B: CENTER OF MASS DYNAMICS

In this section we analyze autocorrelation of the center of mass velocity vector, focusing on the speed $v_s(t)$ and orientation $\theta(t)$ separately. Here we distinguish between the direct measures of the correlation times t_s and t_θ associated with multiexponential decays of correlations, from the assumptions of single exponential decays with τ_s, τ_θ used in the analysis of dynamical crossovers in Sec. III F. In Fig. 9 we show the autocorrelation of speed, $C_{v_s}(t) = \langle \delta v_s(t) \delta v_s(0) \rangle / \langle \delta v_s^2 \rangle$. A fast single exponential decay $\exp(-t/t_s)$ is observed at both Pe = 1, 10, with $t_s \approx 0.1\tau, 1.0\tau$, respectively. However, at Pe = 100, we observe multiple exponential decays with time scales $t_s \approx 1\tau, 250\tau, 3600\tau$ (see the inset of Fig. 9).

The orientational correlation $C_\theta(t) = \langle e^{i[\theta(t)-\theta(0)]} \rangle$ shows multiple exponential decays at all Pe values (Fig. 10). The initial decay is fast with $t_\theta \approx 1\tau$. For Pe = 1, 10 we can extract the longer time scales, as shown in the log-log plot in the inset for Pe = 1, to give $t_\theta = 1500\tau, 2000\tau$, respectively. However, for Pe = 100, in the absence of better averaging, it is difficult to extract the longest time scale.

Moreover, the speed and orientations remain correlated. The cross-correlation functions $C_{v_s,\theta}(t) = \langle v_s(t)\theta(0) \rangle / [\sqrt{\langle \delta v_s^2 \rangle} \sqrt{\langle \delta \theta^2 \rangle}]$ calculated for Pe = 1, 10, 100 are shown in Fig. 11. All of them show significant correlation, which remarkably do not decay with increasing time gap. The asymmetry of the data around $t = 0$ captures the breakdown of time-reversal symmetry due to the nonequilibrium molecular motor drive.

[1] J. Howard, *Mechanics of Motor Proteins and the Cytoskeleton* (Oxford University Press, New York, 2005).

[2] B. Alberts, D. Bray, K. Hopkins, A. Johnson, J. Lewis, M. Raff, K. Roberts, and P. Walter, *Essential Cell Biology* (Garland Science, New York, 2014).

[3] R. D. Vale, Cell **112**, 467 (2003).

[4] D. Chowdhury, Phys. Rep. **529**, 1 (2013).

[5] W. O. Hancock and J. Howard, Proc. Natl. Acad. Sci. USA **96**, 13147 (1999).

[6] D. A. Fletcher and R. D. Mullins, Nature (London) **463**, 485 (2010).

[7] F. Huber, J. Schnauß, S. Rönicke, P. Rauch, K. Müller, C. Fütterer, and J. Käs, Adv. Phys. **62**, 1 (2013).

[8] F. C. MacKintosh, J. Käs, and P. A. Janmey, Phys. Rev. Lett. **75**, 4425 (1995).

[9] H. Yamaoka, S. Matsushita, Y. Shimada, and T. Adachi, Biomech. Model. Mechanobiol. **11**, 291 (2012).

[10] F. H. Kreten, C. Hoffmann, D. Riveline, and K. Kruse, Phys. Rev. E **98**, 012413 (2018).

[11] S. J. Kron and J. A. Spudich, Proc. Natl. Acad. Sci. USA **83**, 6272 (1986).

[12] K. Sekimoto, N. Mori, K. Tawada, and Y. Y. Toyoshima, Phys. Rev. Lett. **75**, 172 (1995).

[13] T. Surrey, F. Nédélec, S. Leibler, and E. Karsenti, Science **292**, 1167 (2001).

[14] V. Schaller, C. Weber, C. Semmrich, E. Frey, and A. R. Bausch, Nature (London) **467**, 73 (2010).

[15] Y. Sumino, K. H. Nagai, Y. Shitaka, D. Tanaka, K. Yoshikawa, H. Chaté, and K. Oiwa, Nature (London) **483**, 448 (2012).

[16] L. Bourdieu, T. Duke, M. B. Elowitz, D. A. Winkelmann, S. Leibler, and A. Libchaber, Phys. Rev. Lett. **75**, 176 (1995).

[17] J. Kierfeld, K. Frentzel, P. Kraikivski, and R. Lipowsky, Eur. Phys. J. Spec. Top. **157**, 123 (2008).

[18] K. Oiwa, S. Chaen, E. Kamitsubo, T. Shimmen, and H. Sugi, Proc. Natl. Acad. Sci. USA **87**, 7893 (1990).
[19] D. L. Coy, M. Wagenbach, and J. Howard, J. Biol. Chem. **274**, 3667 (1999).
[20] A. D. Mehta, R. S. Rock, M. Rief, J. A. Spudich, M. S. Mooseker, and R. E. Cheney, Nature (London) **400**, 590 (1999).
[21] M. Rief, R. S. Rock, A. D. Mehta, M. S. Mooseker, R. E. Cheney, and J. A. Spudich, Proc. Natl. Acad. Sci. USA **97**, 9482 (2000).
[22] M. J. Schnitzer, K. Visscher, and S. M. Block, Nat. Cell Biol. **2**, 718 (2000).
[23] R. S. Rock, S. E. Rice, A. L. Wells, T. J. Purcell, J. A. Spudich, and H. L. Sweeney, Proc. Natl. Acad. Sci. USA **98**, 13655 (2001).
[24] A. Yildiz, J. N. Forkey, S. A. McKinney, T. Ha, Y. E. Goldman, and P. R. Selvin, Science **300**, 2061 (2003).
[25] S. P. Gross, M. Carolina Tuma, S. W. Deacon, A. S. Serpinskaya, A. R. Reilein, and V. I. Gelfand, J. Cell Biol. **156**, 855 (2002).
[26] C. Kural, H. Kim, S. Syed, G. Goshima, V. I. Gelfand, and P. R. Selvin, Science **308**, 1469 (2005).
[27] F. Jülicher and J. Prost, Phys. Rev. Lett. **75**, 2618 (1995).
[28] A. Vilfan, E. Frey, and F. Schwabl, Eur. Phys. J. B **3**, 535 (1998).
[29] M. Badoual, F. Jülicher, and J. Prost, Proc. Natl. Acad. Sci. USA **99**, 6696 (2002).
[30] S. W. Grill, K. Kruse, and F. Jülicher, Phys. Rev. Lett. **94**, 108104 (2005).
[31] S. Klumpp and R. Lipowsky, Proc. Natl. Acad. Sci. USA **102**, 17284 (2005).
[32] C. Leduc, N. Pavin, F. Jülicher, and S. Diez, Phys. Rev. Lett. **105**, 128103 (2010).
[33] P. Kraikivski, R. Lipowsky, and J. Kierfeld, Phys. Rev. Lett. **96**, 258103 (2006).
[34] A. Nair, S. Chandel, M. K. Mitra, S. Muhuri, and A. Chaudhuri, Phys. Rev. E **94**, 032403 (2016).
[35] F. J. Nédélec, T. Surrey, A. C. Maggs, and S. Leibler, Nature (London) **389**, 305 (1997).
[36] H. Y. Lee and M. Kardar, Phys. Rev. E **64**, 056113 (2001).
[37] S. Sankararaman, G. I. Menon, and P. B. Sunil Kumar, Phys. Rev. E **70**, 031905 (2004).
[38] H. Jiang and Z. Hou, Soft Matter **10**, 9248 (2014).
[39] H. Jiang and Z. Hou, Soft Matter **10**, 1012 (2014).
[40] R. E. Isele-Holder, J. Elgeti, and G. Gompper, Soft Matter **11**, 7181 (2015).
[41] R. Chelakkot, A. Gopinath, L. Mahadevan, and M. F. Hagan, J. R. Soc. Interface **11**, 20130884 (2014).
[42] G. Jayaraman, S. Ramachandran, S. Ghose, A. Laskar, M. S. Bhamla, P. B. S. Kumar, and R. Adhikari, Phys. Rev. Lett. **109**, 158302 (2012).
[43] A. Laskar, R. Singh, S. Ghose, G. Jayaraman, P. B. S. Kumar, and R. Adhikari, Sci. Rep. **3**, 1964 (2013).
[44] D. Sarkar and S. Thakur, J. Chem. Phys. **146**, 154901 (2017).
[45] D. Sarkar and S. Thakur, Phys. Rev. E **93**, 032508 (2016).
[46] D. Sarkar, S. Thakur, Y.-G. Tao, and R. Kapral, Soft Matter **10**, 9577 (2014).
[47] K. R. Prathyusha, S. Henkes, and R. Sknepnek, Phys. Rev. E **97**, 022606 (2018).
[48] Ö. Duman, R. E. Isele-Holder, J. Elgeti, and G. Gompper, Soft Matter **14**, 4483 (2018).
[49] N. Kikuchi, A. Ehrlicher, D. Koch, J. A. Käs, S. Ramaswamy, and M. Rao, Proc. Natl. Acad. Sci. USA **106**, 19776 (2009).
[50] J. Gladrow, N. Fakhri, F. C. MacKintosh, C. F. Schmidt, and C. P. Broedersz, Phys. Rev. Lett. **116**, 248301 (2016).
[51] T. Eisenstecken, G. Gompper, and R. Winkler, Polymers (Basel) **8**, 304 (2016).
[52] A. Ghosh and N. S. Gov, Biophys. J. **107**, 1065 (2014).
[53] É. Fodor, C. Nardini, M. E. Cates, J. Tailleur, P. Visco, and F. van Wijland, Phys. Rev. Lett. **117**, 038103 (2016).
[54] C. Ganguly and D. Chaudhuri, Phys. Rev. E **88**, 032102 (2013).
[55] D. Chaudhuri, Phys. Rev. E **90**, 022131 (2014).
[56] A. Dhar and D. Chaudhuri, Phys. Rev. Lett. **89**, 065502 (2002).
[57] Y. Yang, V. Marceau, and G. Gompper, Phys. Rev. E **82**, 031904 (2010).
[58] A. Chaudhuri and D. Chaudhuri, Soft Matter **12**, 2157 (2016).
[59] M. Rubinstein and R. H. Colby, *Polymer Physics* (Oxford University Press, Oxford, 2003).
[60] C. Leduc, O. Campàs, K. B. Zeldovich, A. Roux, P. Jolimaitre, L. Bourel-Bonnet, B. Goud, J.-F. Joanny, P. Bassereau, and J. Prost, Proc. Natl. Acad. Sci. USA **101**, 17096 (2004).
[61] S. M. Block, L. S. B. Goldstein, and B. J. Schnapp, Nature (London) **348**, 348 (1990).
[62] R. D. Vale, T. Funatsu, D. W. Pierce, L. Romberg, Y. Harada, and T. Yanagida, Nature (London) **380**, 451 (1996).
[63] D. Chaudhuri, Phys. Rev. E **75**, 021803 (2007).
[64] S. G. Krantz, *Handbook of Complex Variables* (Birkhäuser, Boston, MA, 1999).
[65] F. Peruani and L. G. Morelli, Phys. Rev. Lett. **99**, 010602 (2007).
[66] D. Selmeczi, S. Mosler, P. H. Hagedorn, N. B. Larsen, and H. Flyvbjerg, Biophys. J. **89**, 912 (2005).
[67] Given that both mass and viscous friction scale similarly with the chain length, $\tau_I = 1$.

Correction: The first sentence of the abstract contained an error in wording and has been corrected.